Defect-Passivated $InGaZnO/In_2O_3$ Stacked Thin-Film Transistor with Visible-Light-Assisted Recovery for Room-Temperature ppb-Level NO_2 Detection

Chengyao Liang,[a] Wei Hu,[a] Di Peng,*[b] Yong Zhou,[a] Yong Wang,[c] Yi Guo,[c] Peng Zhang,[c] Yuhong Wu,[c] Xi Yang*[d] and Yong He*[a]

a Key Laboratory of Optoelectronic Technology and Systems of the Education Ministry of China, College of Optoelectronic Engineering, Chongqing University, Chongqing 400044, China

b Chongqing Institutes of Higher Education Key Forensic Science Laboratory, Criminal Investigation School, Southwest University of Political Science and Law, Chongqing 401120, China

c Chongqing Key Laboratory of Toxic and Drug Analysis, Chongqing Police College, Chongqing 401331, China

d Institute of Chemical Materials, China Academy of Engineering Physics, Mianyang 621900, China

***: Corresponding Authors**

Email addresses:

pengdi@swupl.edu.cn (D. Peng), xyang@caep.cn (X. Yang) and yonghe@cqu.edu.cn (Y. He).

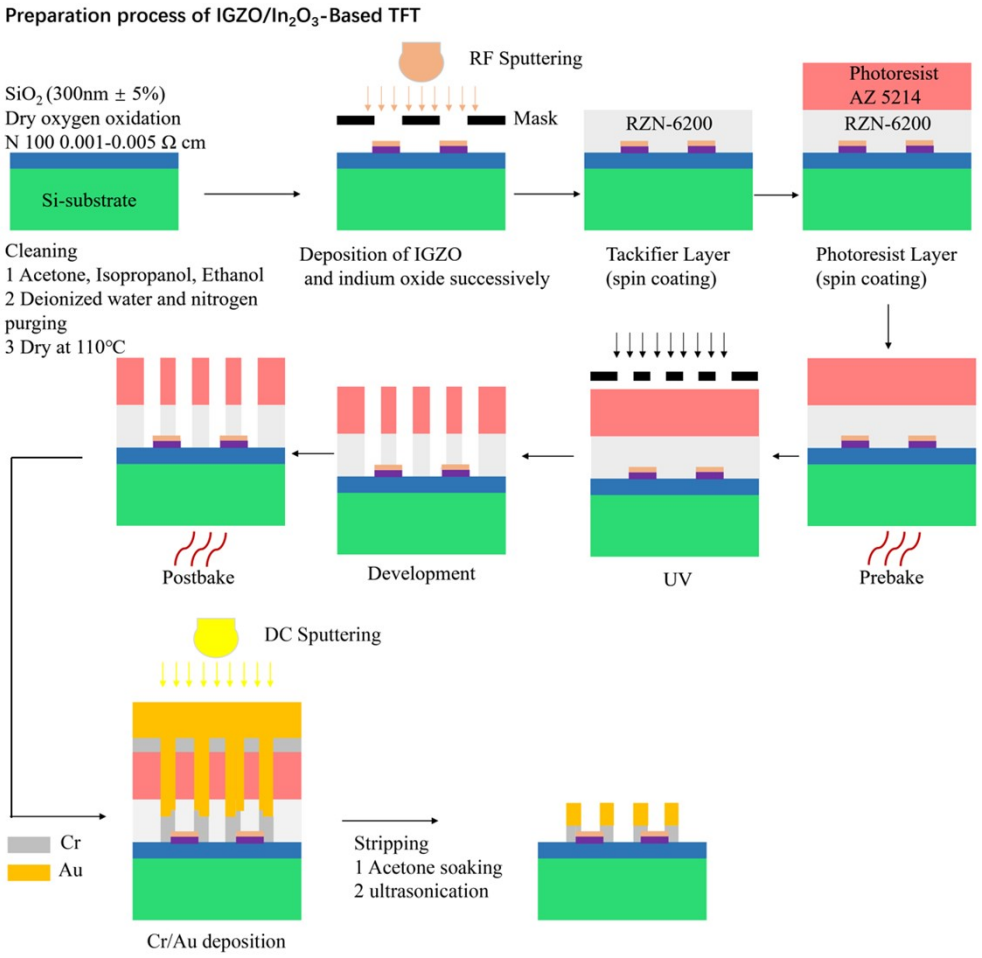

Fig. S1. The preparation process of the IGZO/In_2O_3 TFT through a bottom-up process.

Table S1. PBS stability of the In_2O_3 TFT.

PBS duration (min)	0	5	10	30	60
Threshold voltage (V)	-15.28 ± 0.60	-14.90 ± 0.62	-14.46 ± 0.73	-13.85 ± 0.82	-13.03 ± 0.78
Saturated on-state current (μA)	96.85 ± 7.92	96.31± 6.78	96.10 ± 6.63	93.64 ± 8.95	91.79 ± 9.13

Table S2. PBS stability of the IGZO/In_2O_3 TFT.

PBS duration (min)	0	5	10	30	60
Threshold voltage (V)	1.70 ± 0.58	1.88 ± 0.55	2.01 ± 0.72	2.19 ± 0.69	2.38 ± 0.67
Saturated on-state current (μA)	296.47 ± 17.79	291.05 ± 20.61	286.81 ± 19.46	280.57 ± 22.38	277.12 ± 23.20

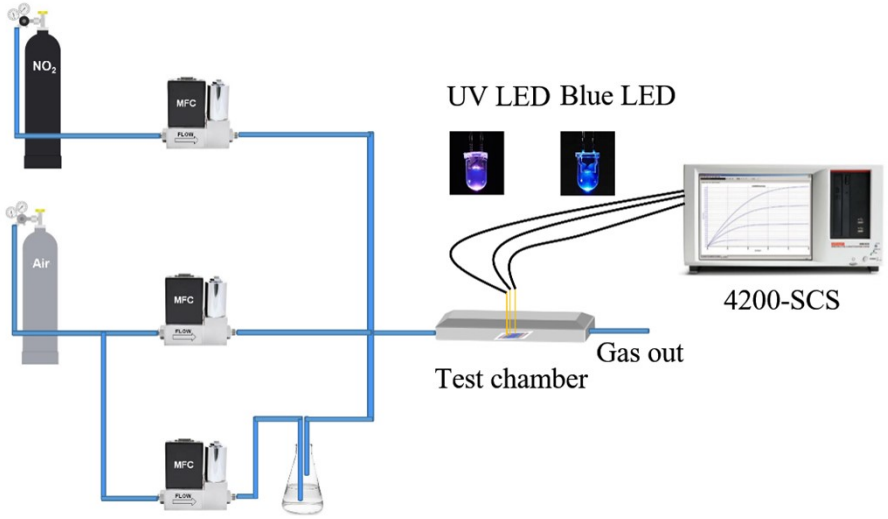

Fig. S2. The configuration for gas sensing of the prepared In_2O_3 and IGZO/In_2O_3 TFTs.

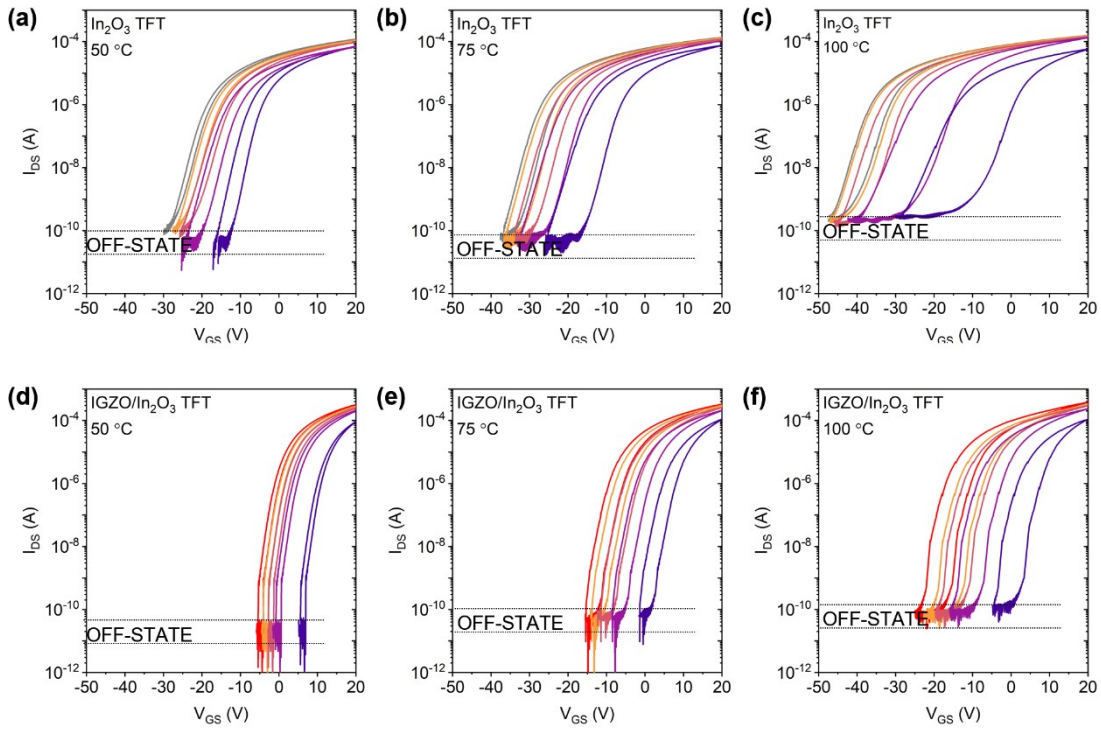

Fig. S3. Hysteresis curves composed of forward and backward transfer characteristics of In_2O_3 TFTs at (a) 50°C, (b) 75°C and (c) 100°C under 50-500 ppb NO_2 concentrations. Corresponding hysteresis curves of IGZO/In_2O_3 TFTs at (d) 50°C, (e) 75°C and (f) 100°C.

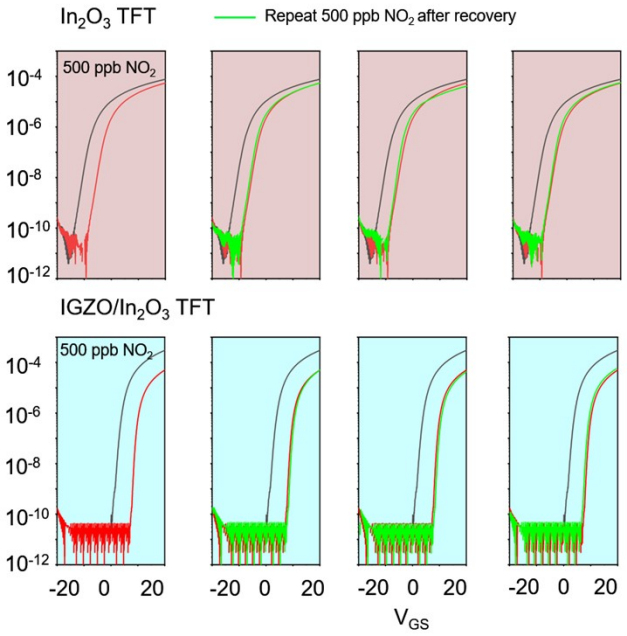

Fig. S4 Transfer characteristics of In_2O_3 TFT and IGZO/In_2O_3 TFT, tested repeatedly for 500 ppb NO_2 gas sensing, showing the response after exposure to 500 ppb NO_2 and subsequent recovery following UV or Blue LED stimulation.

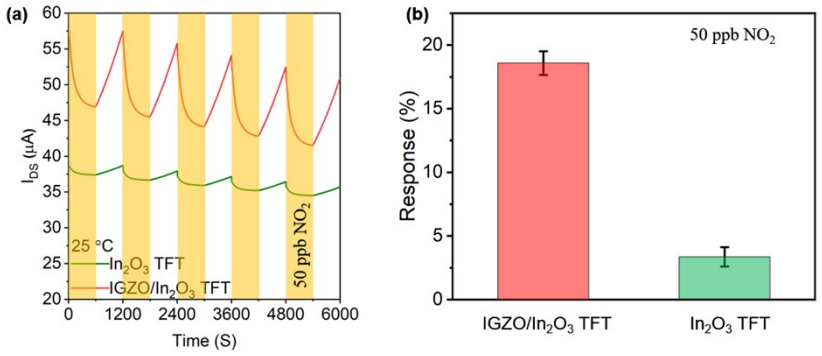

Fig. S5. (a) Dynamic response to 50 ppb NO_2 for 5 consecutive cycles at room temperature of the In_2O_3 and IGZO/In_2O_3 TFT with V_G and V_D fixing at 10 V and 1 V, respectively. (b) Mean and standard deviation of response values of In_2O_3 and IGZO/In_2O_3 TFT to 50 ppb NO_2 for 5 consecutive cycles at 25 °C.

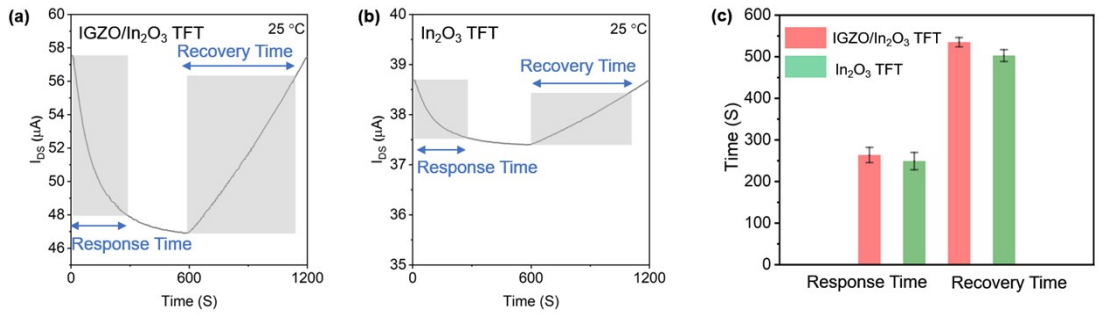

Fig. S6. (a) In_2O_3, and (b) IGZO/In_2O_3 TFT: A typical sensing cycle in response to 50 ppb NO_2. (c) Response and recovery times statistically calculated from five consecutive 50 ppb NO_2 sensing cycles.

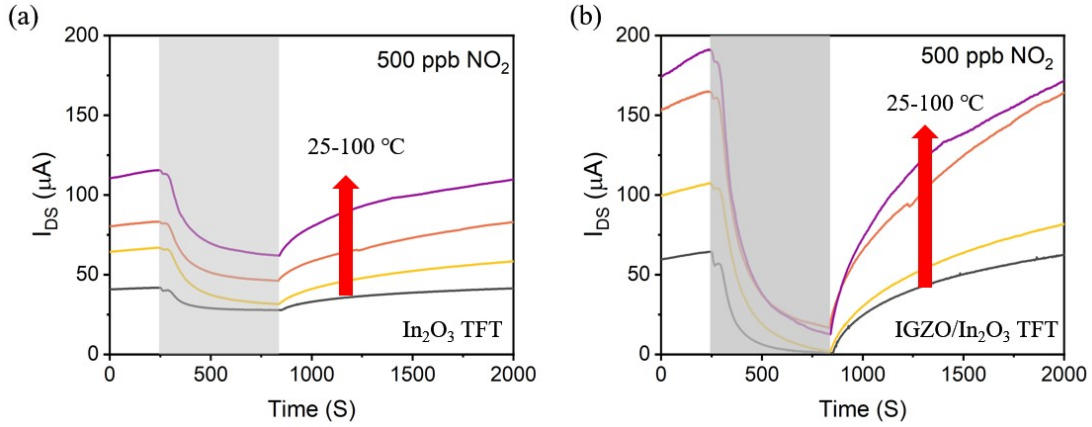

Fig. S7. Dynamic response to 500 ppb NO_2 of the In_2O_3 and IGZO/In_2O_3 TFT with V_G and V_D fixing at 10 V and 1 V, respectively.

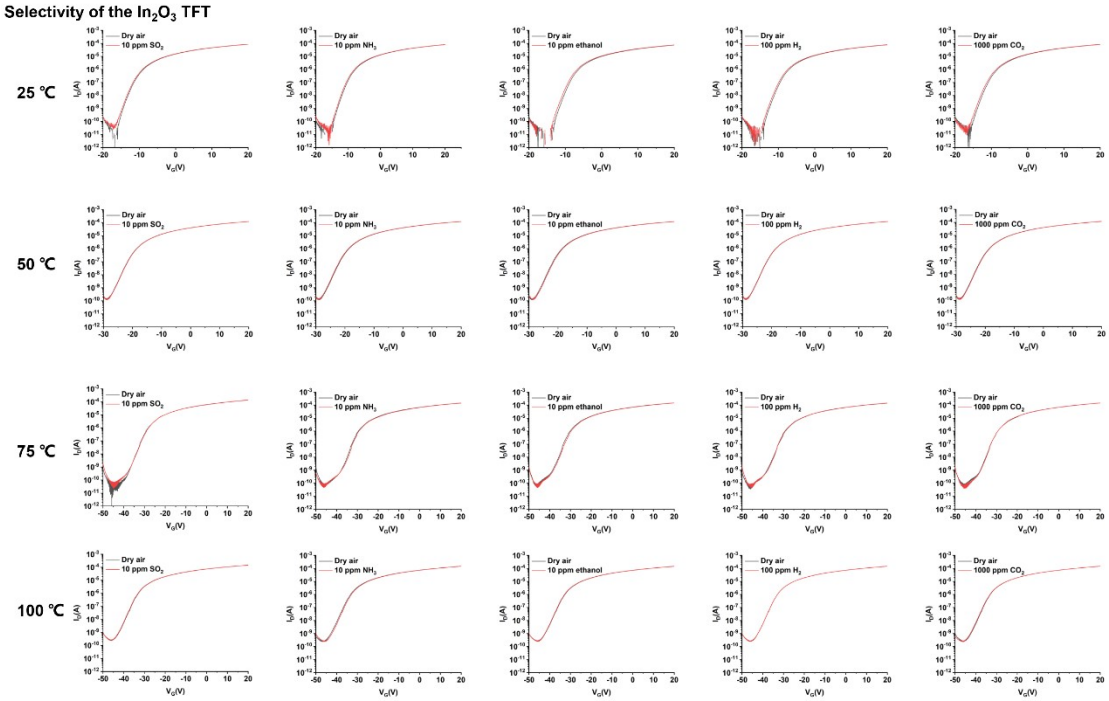

Fig. S8. The selectivity of the In_2O_3 TFT.

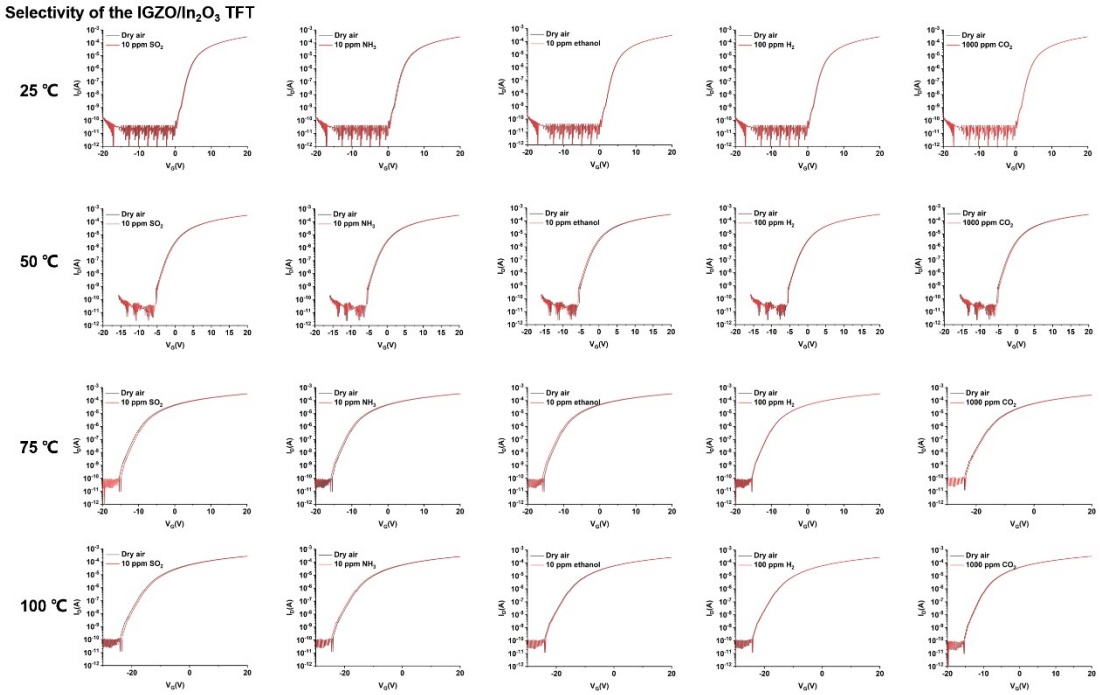

Fig. S9. The selectivity of the IGZO/In_2O_3 TFT.

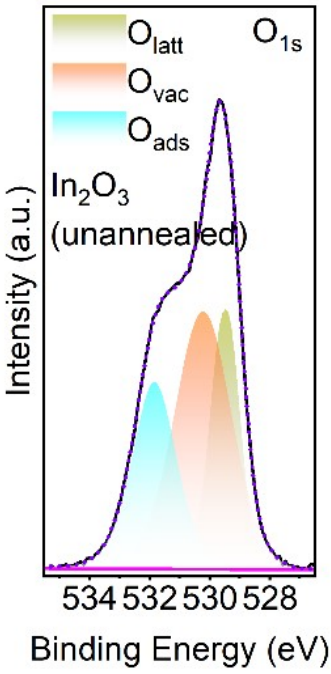

Fig. S10 The O 1s spectra corresponding to the unannealed In_2O_3 thin film.

Table S3. Detailed electrical parameters of In_2O_3 TFT after response to 50-500 ppb NO_2.

	Unexposed	50 ppb NO_2	100 ppb NO_2	200 ppb NO_2	500 ppb NO_2
μ_{FE} (cm^2/Vs)	7.55 ± 0.35	7.26 ± 0.68	6.83 ± 0.45	6.53 ± 0.56	5.82 ± 0.70
Vth (V)	-15.28 ± 0.60	-14.58 ± 0.52	-14.28 ± 0.50	-13.78 ± 0.57	-10.08 ± 0.84
On-state current ($\times 10^{-5}$A)	7.74 ± 0.36	7.62 ± 0.43	7.12 ± 0.33	6.88 ± 0.71	5.45 ± 0.61
Off-state current ($\times 10^{-11}$A)	1.78 ± 1.03	1.41 ± 0.94	1.29 ± 0.86	0.61 ± 0.59	0.37 ± 0.25

Table S4. Detailed electrical parameters of IGZO/In_2O_3 TFT after response to 50-500 ppb NO_2.

	Unexposed	50 ppb NO_2	100 ppb NO_2	200 ppb NO_2	500 ppb NO_2
μ_{FE} (cm^2/VS)	18.79 ± 0.83	18.06 ± 0.98	17.37 ± 1.26	10.74 ± 1.52	7.14 ± 1.13
Vth (V)	1.70 ± 0.58	2.70 ± 0.50	3.60 ± 0.43	5.11 ± 0.77	6.67 ± 0.91
On-state current ($\times 10^{-4}$A)	2.99 ± 0.14	2.85 ± 0.17	2.49 ± 0.12	1.25 ± 0.26	0.49 ± 0.06
Off-state current ($\times 10^{-11}$A)	2.51 ± 1.45	2.39 ± 1.33	2.09 ± 1.21	1.04 ± 1.08	0.71 ± 0.35

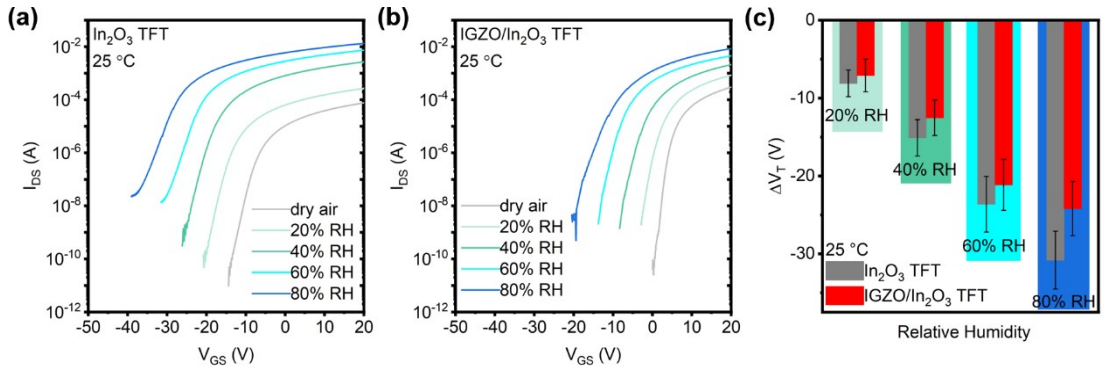

Fig. S11. The transfer characteristics of the (a) In_2O_3 and (b) IGZO/In_2O_3 TFTs under 20-80% RH conditions at room temperature. (c) The statistics of ΔV_T that compared to V_T measured in dry air.

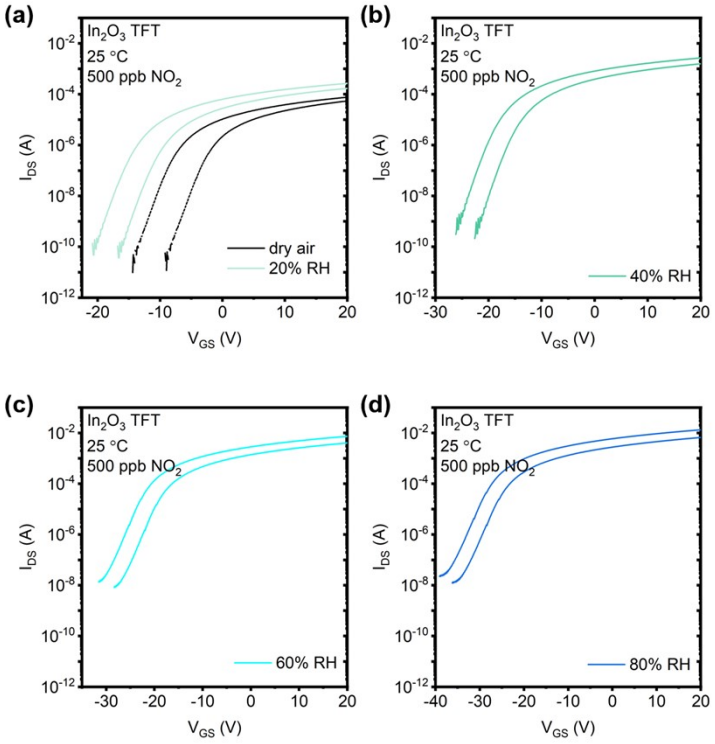

Fig. S12. (a) The response of the In_2O_3 TFTs towards 500 ppb NO_2 under dry air, 20% RH, (b) 40% RH, (c) 60% RH, and (d) 80% RH.

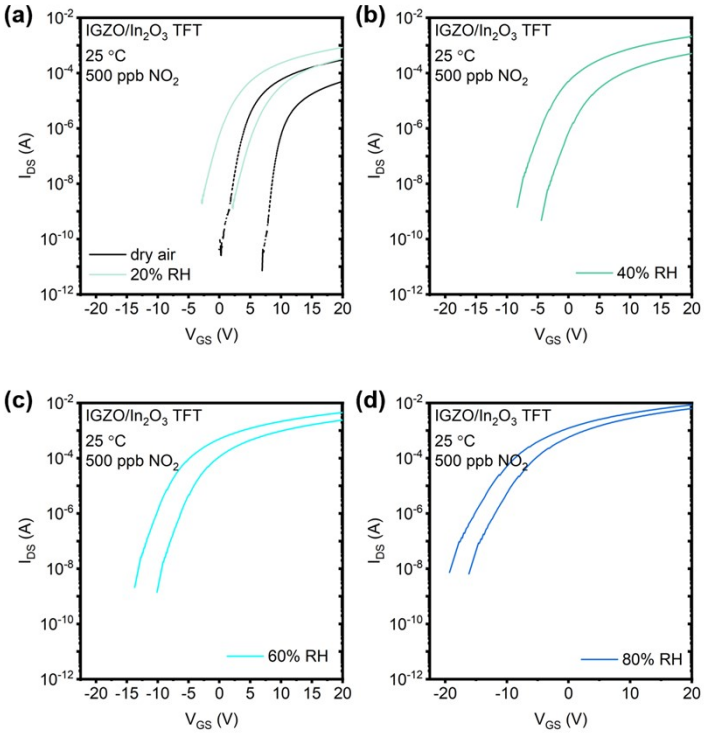

Fig. S13. (a) The response of the IGZO/In_2O_3 TFTs towards 500 ppb NO_2 under dry air, 20% RH, (b) 40% RH, (c) 60% RH, and (d) 80% RH.

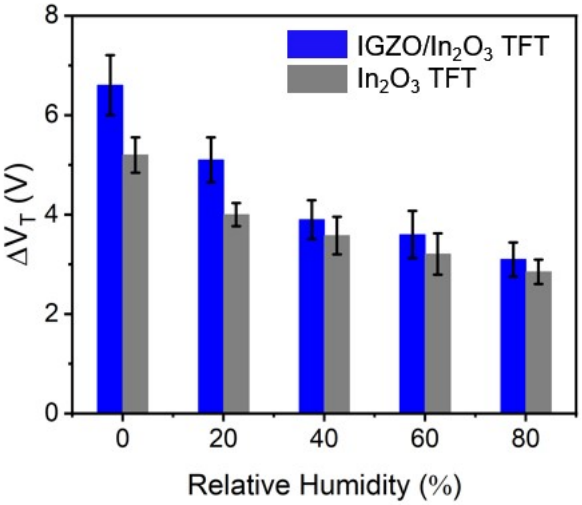

Fig. S14. A summary of ΔV_T of the In_2O_3 and IGZO/In_2O_3 TFTs towards 500 ppb NO_2 under 20-80% RH at room

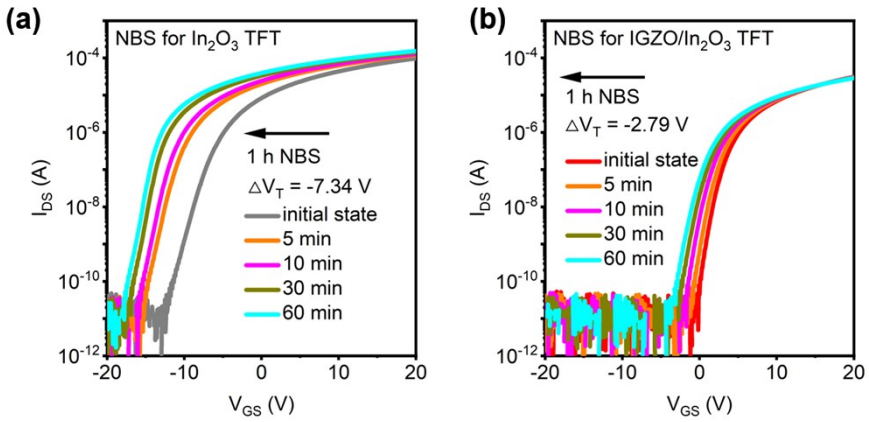

Fig. S15. NBS stability under the condition of fixed V_{GS}= -20 V and V_{DS}=1 V within 60 minutes of (a) In_2O_3 TFTs and (b) IGZO/In_2O_3 TFTs.

Table S5. Comparison of sensing performance based on metal oxide field effect transistor gas sensors.

	Sensor fabrication	NO_2 Conc. (ppb)	Response (Ra-Rg)/Ra	Temperature (℃)	Ref.
Hydroxy-Rich-Surface In_2O_3 FET	RF magnetron sputtering	500	~2500%	100	[46]
O-deficient In_2O_3 TFT	RF magnetron sputtering	100	~21.4%	160	[47]
Floating-gate In_2O_3 FET	RF magnetron sputtering	500	~1800%	100	[48]
Floating-gate In_2O_3 TFT	RF magnetron sputtering	300	~69%	75	[49]
SnO FET	Liquid metal method	500	~20%	RT	[50]
IGZO FET	RF magnetron sputtering	10	~18%	~150	[51]
$Ni_3(HHTP)_2$ FET	In-situ grown	100	~21.5%	RT	[52]
IGZO/In_2O_3 TFT	RF magnetron sputtering	50	~18.6%	RT	This work

NBS characteristics of In_2O_3 TFT and IGZO/In_2O_3 TFT. V_{GS} was set to -20 V, and V_{DS} was maintained at 1 V. After 1 hour of NBS stress, the threshold voltage negative shift ΔV_T of In_2O_3 and IGZO/In_2O_3 TFTs were -7.34 V and -2.79 V, respectively, as shown in Figure S9. This indicates that the threshold voltage drift of the IGZO/In_2O_3 TFT under negative bias stress is significantly smaller than that of the In_2O_3 TFT. This suggests that the IGZO/In_2O_3 TFT experiences less performance degradation and has better stability. Compared to the IGZO/In_2O_3 TFT, the defects in the oxide semiconductor film of the In_2O_3 TFT are more easily activated under negative bias. In_2O_3, as a single material, have more intrinsic defects, and these defect states can quickly capture charge carriers under negative bias, resulting in a significant shift in

threshold voltage. On the other hand, the IGZO/In_2O_3 TFT uses a composite structure of IGZO and In_2O_3, which typically exhibits better performance by improving the crystal structure or reducing the formation of certain defects. Overall, the IGZO/In_2O_3 TFT shows better NBS performance, mainly due to its composite film structure, which effectively reduces defect formation and the degradation effect of negative bias on device performance, maintaining better electrical stability and long-term reliability. In contrast, the In_2O_3 TFT, with more defect states, experiences more severe performance degradation under negative bias.

The origin of PBS and the significance of PBS testing. Positive bias stress (PBS) is of significance in thin-film transistor technology and PBS testing serves as a method to evaluate the stability and reliability of TFT devices over prolonged operational durations [42-44]. It becomes feasible to simulate voltage stresses that the devices might encounter during real-world usage, such as prolonged operation or stresses induced by specific environmental conditions by subjecting TFTs to positive bias stress. These TFTs exhibited a trend of threshold voltage positive shift and gradual decrease in drain current and two reasons account for this phenomenon. Firstly, lattice mismatch occurring at the interface between In_2O_3 or IGZO thin film layer and the insulating layer SiO_2, inevitably leads to defect states such as unsaturated dangling bonds. Part free electrons are captured by interface defect states under PBS conditions, resulting in a reduction in the concentration of free electrons in the channel layer [40]. Therefore, additional gate voltage, i.e., an increase in threshold voltage ΔV_T, is required to

overcome the effects caused by these captured electrons, thereby mitigating the positive drift of threshold voltage and decrease in drain current. Secondly, the sensing layer In_2O_3 is highly sensitive to oxygen due to its strong electronegativity, and the oxygen adsorbed on the thin film surface captures electrons from the channel layer surface. The reaction equation during low-temperature measurements (below 100°C) is as follows:

$$O_2 + e^- \rightarrow O_2^- \#(1)$$

Under the combined influence of oxygen in the air and interface defect states, the electron concentration in the channel of the fabricated depletion-type thin-film transistors (DTFTs) is reduced, resulting in a decrease in the additional negative voltage required to deplete electrons, thereby causing the threshold voltage to shift forward.

The influence of temperature on output current and NO_2 sensing. In_2O_3 and IGZO/In_2O_3 TFTs are both n-type transistors. First, the concentration of free electrons increases with rising temperature because the thermal excitation effect causes more electrons to transition from the valence band to the conduction band, thereby enhancing the electrical conductivity. Second, at lower temperatures, the mobility of charge carriers in the semiconductor material is relatively low due to the higher scattering frequency of carriers within the channel, which results in lower conductivity. As the temperature increases, the motion of charge carriers becomes more active, scattering events decrease, and mobility improves. These two factors contribute to an increase in leakage current. Additionally, the negative shift in threshold voltage can be attributed

to the increased number of free carriers, which allows the device to conduct at a lower gate voltage. NO_2 molecules interact with the surface of n-type semiconductors, capturing surface free electrons and reducing the electron concentration in the channel, which consequently decreases its conductivity. This phenomenon serves as the foundation for NO_2 gas sensing. Specifically, a higher concentration of NO_2 results in the capture of more electrons, leading to a more significant reduction in conductivity. This change manifests in two prominent ways, a positive shift in the threshold voltage and a decrease in the output current.